Annealing effects in ferroelectric poly-(vinylidene fluoride–trifluoroethylene) copolymers: real-time studies using synchrotron radiation

C. Bourgaux-Leonard
LURE (CNRS-CEA), Universite de Paris-Sud, 91405 Orsay Cedex, France

and J.F. Legrand*
Institut Laue-Langevin, BP 156X, 38042 Grenoble, France

and A. Renault and P. Delzenne†
Laboratoire de Spectrometrie Physique (associe au CNRS), Universite J. Fourier Grenoble, BP 87, 38402 Saint Martin d'Heres Cedex, France
(Received 23 May 1990; revised 10 September 1990; accepted 1 October 1990)

Poly(vinylidene fluoride–trifluoroethylene) ($P(VF_2$–TrFE)) copolymers with about 30 mol% of TrFE exhibit a ferroelectric transition of first-order type around 100°C. This transition is investigated using complementary measurements of small angle X-ray scattering and wide angle X-ray diffraction. The results provide information on the properties of both the amorphous and crystalline phases as a function of temperature and on the lamellar morphology. They show that temperature cycling through the Curie transition increases the degree of crystallinity of the polymer and modifies the structure.

(Keywords: vinylidene fluoride–trifluoroethylene copolymers; ferroelectric phase transition; X-ray diffraction; small angle X-ray scattering)

INTRODUCTION

Random copolymers of vinylidene fluoride (CH_2–CF_2 or VF_2) and trifluoroethylene (CHF–CF_2 or TrFE), with VF_2 content ranging from 60 to 80 mol%, are the first polymers whose crystalline phase exhibits a clear ferroelectric transition upon heating above room temperature[1–4].

The crystallized regions are embedded in an amorphous matrix which is made of chain folds at the surface of the lamellar crystals, cilia, links between lamellae, entanglements and defects along the chain expelled from the crystalline regions, etc.

In the ferroelectric crystal phase the chains have a planar *trans–trans* conformation, the same as in stretched β-PVF_2 (space group *Cm2m*). This allows parallel alignment of the molecular dipole moments and results in a large spontaneous polarization (110 mC m^{-2} for 70% VF_2 content).

At the Curie temperature, T_c, which increases from 78 to 140°C when the VF_2 content is increased from 60 to 80 mol%, this conformation transforms into random sequences of *TG*, *TG'* and *TT* units (centrosymmetric space group *6/mmm*). The dipole moments are thus orientationally disordered around the chain axis[4–6]. Both the polarization and the piezoelectric activity drop to zero above T_c.

Nuclear magnetic resonance (n.m.r.) and neutron scattering studies demonstrate the dynamic character of this conformational disorder: the polymer chains exhibit large amplitude motion in the expanded paraelectric lattice[7–10]. This high mobility is expected to induce lamellar thickening, increase the overall degree of crystallinity and reorganization of the microstructure through T_c.

We report here the effect of temperature cycles on the lamellar structure of a 70/30 mol% VF_2–TrFE copolymer. This investigation is based on wide angle and small angle X-ray diffraction using synchrotron radiation (SR). The small divergence of the SR permits high resolution measurements and its high brilliance allows real-time investigations to be made especially during the phase transition.

The proportions of amorphous, ferroelectric and paraelectric phases, the evolution of the lattice parameters as functions of temperature and the coherence length of the crystalline regions can be obtained from the Bragg reflections at wide angles.

Small angle X-ray scattering (SAXS) is used to analyse the changes in morphology. The difference in density between the crystalline and the amorphous regions gives rise to scattering at small angles, whose integrated intensity is related to microstructural parameters (volume fraction of the crystalline phase, densities of the crystalline and amorphous phases). The SAXS patterns of semi-crystalline polymers also show a correlation peak. It is usually assumed that this scattering maximum arises

* To whom correspondence should be addressed
† Present address: Shell Chem. Research Centre, Louvain la Neuve, 1348 Belgium

0032-3861/91/040597-08

from spatial correlation of the lamellae. A Bragg spacing can thus be derived, which gives an estimate of the average distance between crystalline lamellae.

EXPERIMENTAL

Samples

The random copolymer of VF_2 and TrFE with mean molecular composition 70/30 was synthesized by Atochem (Pierre Bénite, France). From the raw material two kinds of samples were prepared: unoriented plates, pressed in the melt and then quenched in cold water; and stretched films obtained by rolling unoriented plates (draw ratio 3.5/1).

X-ray apparatus

The key component of the X-ray instrument is a fixed exit, double crystal monochromator (Si or Ge crystals), which provides a beam of narrow energy bandpass ($\Delta E/E \leqslant 10^{-3}$) in the wavelength range 0.8–3 Å. The beam size and the resolution are determined by collimation slits downstream from the monochromator (typically 0.3 × 1.5 mm).

In order to reduce the parasitic scattering, especially at small angles, the beam path is kept under vacuum and antiparasitic slits are placed before the sample. Two almost transparent detectors, placed before and after the sample, permit monitoring of the beam intensity and sample absorption.

The scattering profiles are recorded with a gas-filled (Xe–20% CO_2) position-sensitive detector (one-dimensional). A beam stop of variable width protects the detector from receiving the direct beam. The electronically treated signals are sent into a multichannel analyser and then stored by a microcomputer. The sample-to-detector distance and the wavelength can be adjusted in order to cover different scattering vector ranges, to improve the resolution or to increase the acceptance angle of the detector.

A blank scattering curve, scaled for the difference in absorption, was subtracted from all the sample scattering curves.

Two cycles of heating and cooling were performed on samples initially quenched from the melt in order to separate the effect of the Curie transition from the effect of annealing. The samples were heated stepwise through the transition in a Mettler FP oven set in the beam path. Far from T_c, after a step of 5 K, thermal equilibrium was reached after about 2 min (there was no more change in the scattered intensity after 2 min).

After the same temperature step, but within the region of the Curie transition, the scattered intensity still changed after 10 min. *Figure 1* shows a typical time evolution of the intensity scattered at small angle after a temperature step of −5 K (at $t = 0$). This result confirms the importance of kinetic effects for temperature drifts larger than 1 K min^{-1} (like those of differential scanning calorimetry). In order to minimize these effects during the temperature cycles reported here, we chose to make systematic steps of 5 K every 10 min and to start the measurements after standing for 6 min close to T_c or 3 min far from T_c.

Density measurements

The average density of the specimen was measured before and after annealing by immersion in a gradient density column.

For the quenched samples the density, $\rho = 1.86$ g cm^{-3} before annealing and $\rho = 1.90$ g cm^{-3} after annealing.

For the oriented specimens $\rho = 1.87$ g cm^{-3} before annealing and 1.90 g cm^{-3} after annealing.

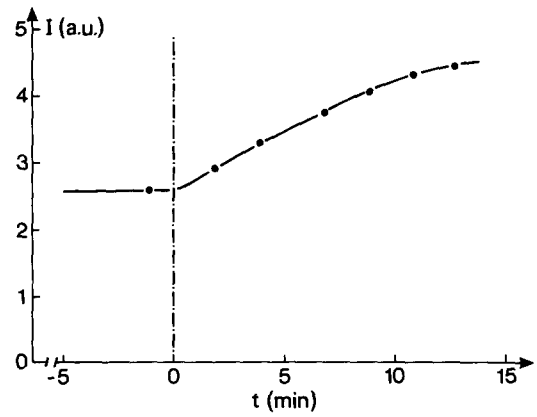

Figure 1 Example of the evolution of the SAXS integrated intensity, I, as a function of time, t, in the Curie transition region, during a cooling run. At $t = 0$ the temperature setpoint was changed from 77 to 72°C

Thermal expansion measurements

The volume changes of the specimens were measured by recording the height of a mercury column in a glass cell in which the sample was immersed, the cell being placed in a temperature-controlled oil bath with programmable drifts. The temperature was measured with a thermocouple and the height of mercury with a displacement transducer of 'LVDT' type. The thermal expansion of the mercury (without sample) was measured for subtraction.

WIDE ANDLE X-RAY DIFFRACTION

Results

At room temperature the polymer exhibits the ferroelectric β-phase which belongs to the orthorhombic symmetry group *Cm2m*. For wavelength, $\lambda = 1.54$ Å, the diffraction pattern (*Figure 2*) shows an intense peak at $2\theta = 19.8°$ which actually consists of two unresolved Bragg reflections (1 1 0) and (2 0 0) according to the pseudo-hexagonal character of the structure. At larger angle, two Bragg peaks much weaker in intensity are observed: in a powder sample, the (0 0 1) at 35.2° merges with the weaker (3 1 0) and (0 2 0) reflections around 34.7°, and the composite (1 1 1) + (2 0 1) reflection at 40.8° merges with the much weaker (4 0 0) and (2 2 0) reflections around 40.1°. Note that this indexing has been obtained from diffraction studies of oriented polymer films[10].

As temperature is increased above 75°C, a peak grows at lower angle ($2\theta = 18°$) indicating the onset of the ferroelectric transition. The two distinct crystal phases: paraelectric and ferroelectric coexist in the temperature range 75–115°C (for the first temperature cycle). Ultimately, at temperatures above 120°C a single narrow peak (paraelectric) is observed at $2\theta = 17.8°$ and only a broad reflection remains around 40°. Texture analysis of oriented specimens prove that it is the (0 0 1) Bragg peak (shifted at larger angle) and that, in the hexagonal paraelectric phase, the other reflections including

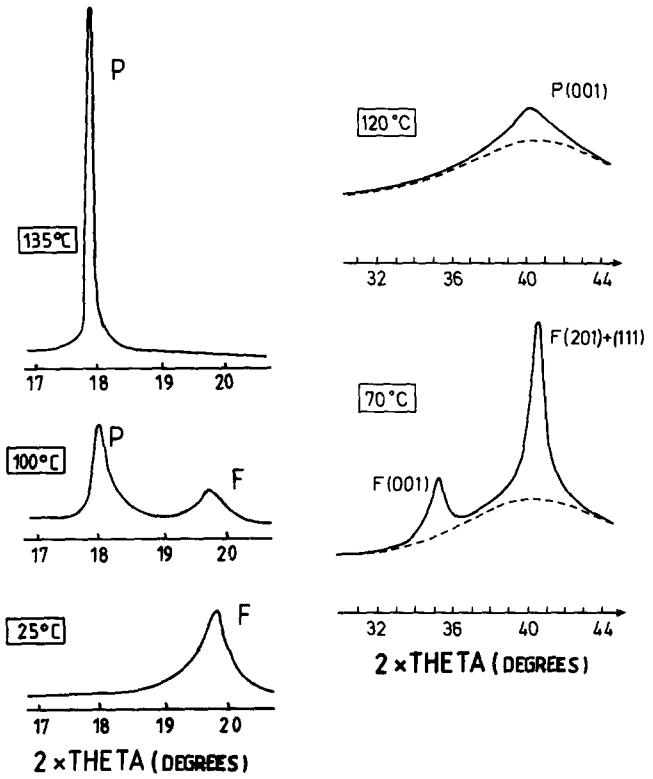

Figure 2 Powder diffraction profiles in the transmission geometry, recorded at different temperatures during a heating run. F, ferroelectric Bragg peaks; P, paralelectric Bragg peaks. Around 40° the dotted line represents an amorphous halo estimated from measurements above the melting point

(1 1 1) + (2 0 1) almost vanish. The transition is reversible on cooling below 70°C. Such a large thermal hysteresis reflects its strong first-order character.

A key feature of the second temperature cycle is the lowering of T_c. The phase transformation starts at 60°C instead of 75°C and the transition is completed at 110°C.

The temperature dependence of the lattice parameters a (or $b\sqrt{3}$) and c is deduced from the positions of the Bragg reflections[10,11]. Upon heating, there is an anomalous expansion of about 9% along the two directions perpendicular to the chain axis and a contraction of about 12% along the -C–C- backbone direction. These are related to the change of the chain conformation: the chain is no longer fully extented as in the ferroelectric phase but its disordered conformation is made of random sequences of TG, TG' and TT units. Therefore the ferro- to paraelectric transition is associated with a large but anisotropic expansion of the lattice ($\Delta V/V = +6\%$, where V is volume). The temperature dependence of the average crystal density ρ_c, deduced from the lattice parameters measurements is shown in *Figure 3*. It is expected that these large volume changes could be accommodated by a modification of the microstructure and by changes in the degree of crystallinity.

An estimate of the overall degree of crystallinity can be obtained from the ratio of the integrated intensities of the amorphous halo and of the crystalline Bragg peaks. Such a determination however requires the separation of these two contributions which are partly superimposed. In order to determine the shape of the amorphous halo, lying below the (1 1 0) + (2 0 0) Bragg peak, we have studied the effect of temperature cycling on a specimen oriented by rolling. In such a sample, the (1 1 0) and (2 0 0) Bragg reflections are concentrated in the equatorial plane while the amorphous halo can be observed almost alone along the meridian direction. One must however note that such an analysis is based on the assumption that the lineshape of the amorphous halo is not much affected by stretching. In a first approximation the halo can be fitted by a Gaussian curve, as shown in *Figure 4a*. The upturn of the experimental curve at high temperature is not observed in the equatorial plane; it is therefore attributed to additional spatial correlations along the chain axis direction. The angular position of the halo slightly decreases with increasing temperature and this reflects the thermal expansion of the amorphous phase. It is also shown in *Figure 4a* that the intensity of the amorphous halo is increased above T_c. This is attributed to a decrease in the degree of crystallinity, χ, in the paraelectric phase.

We have determined χ of pressed samples *versus* temperature during successive heating and cooling runs (*Figure 4b*). Starting with a quenched sample, the first heating run increases χ from 0.65 up to about 0.72 at 120°C. The crystallinity further increases upon cooling: this mainly occurs in the transition region. Such behaviour has already been reported from n.m.r. measurements during temperature cycling[7]. The second temperature cycle results in reversible change of crystallinity ($\chi = 0.73$ above and 0.8 below T_c). The change in χ at room temperature agrees with the increase of the average density from 1.86 to 1.90 g cm^{-3} after annealing.

The total structure factor of the composite (1 1 0) + (2 0 0) Bragg reflection changes through the ferroelectric transition, as shown by the different integrated intensities obtained by neutron and X-ray diffractions[10]. However, from their respective changes with temperature, one can derive the evolution of the relative amount of each phase through the transition. This is shown in *Figure 5*.

Discussion

From the width of the Bragg peaks in the two phases one can get an estimate of the crystalline coherence length L_c using the Scherrer formula:

$$\Delta(2\theta) = 0.9\lambda/L_c \cos\theta$$

In the ferroelectric phase the (1 1 0) and (2 0 0) peaks have a natural width of about 0.5°, from which we infer

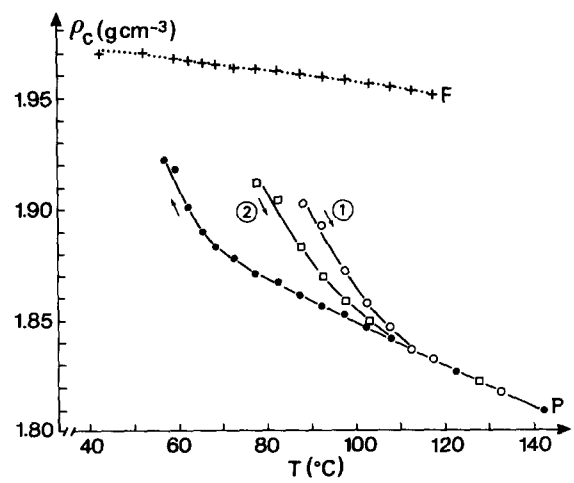

Figure 3 Temperature dependence of the crystal density, ρ_c, through the ferroelectric transition. +, Ferroelectric phase; ○, paraelectric phase, first heating run; □, paraelectric phase, second heating run; ●, paraelectric phase, cooling run

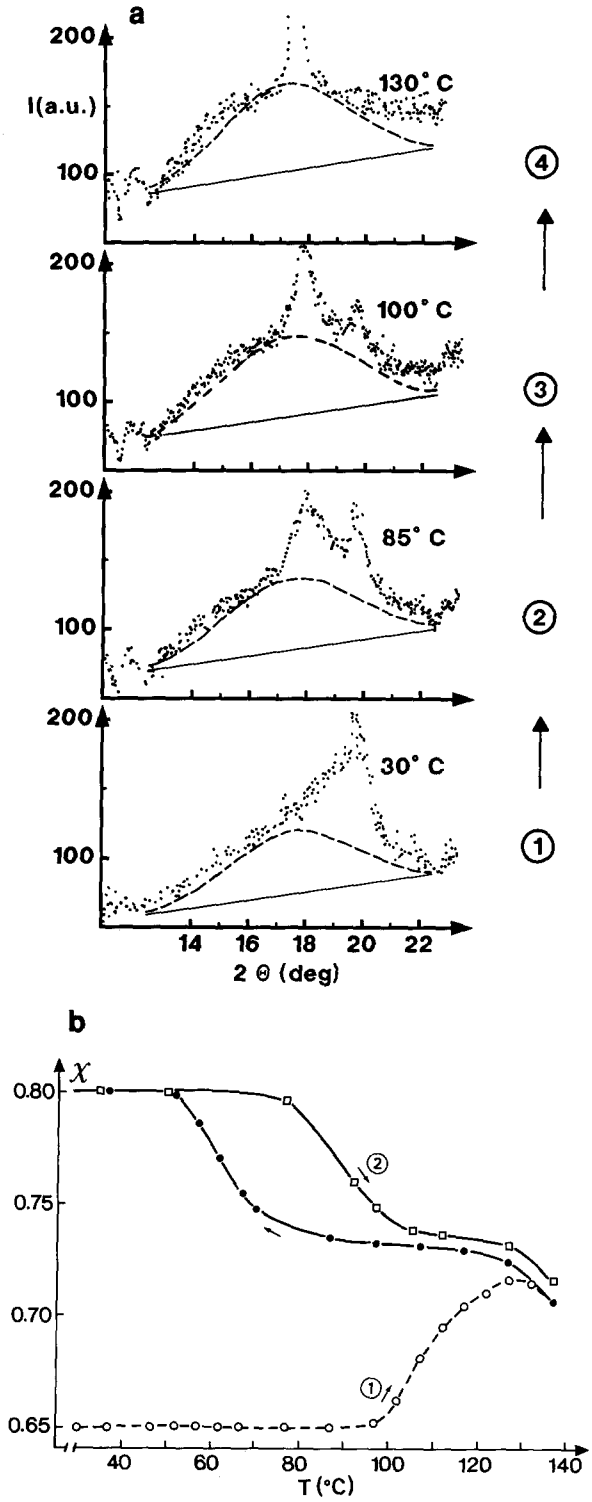

Figure 4 (a) X-ray diffraction patterns, showing the profile of the amorphous halo, recorded with a stretched copolymer along the meridian direction, at different temperatures. (b) Temperature dependence of the degree of crystallinity, χ, during successive heating and cooling runs. ○, First heating run; ●, cooling run; □, second heating run

that the average L_c value is 150 Å along a direction perpendicular to the chain axis c. However, the observation of a (2 0 0) linewidth about twice smaller in polarized samples suggests that 150 Å could be the typical size of a ferroelectric domain inside a crystal with a width of about 300 Å. From the linewidth of the (0 0 1) Bragg peak ($\Delta(2\theta) = 1.0°$), we evaluate the average thickness of the lamellae along the chain axis direction to be 80 Å.

At high temperature, the small width ($\Delta(2\theta) = 0.1°$) of the (1 1 0) + (2 0 0) peak partly comes from the identity of the interplanar distances d_{110} and d_{200} in the hexagonal paraelectric phase, but is also shows that L_c perpendicular to the chain axis c is much larger (about 800 Å). The (0 0 1) peak becomes very broad, corresponding to a L_c of only 35 Å (this value could however be a little overestimated due to the superimposition of the amorphous halo). These results support the two-dimensional character of the structure in the disordered paraelectric phase: the centres of mass of the chains are regularly stacked in a hexagonal lattice, but the conformational changes produce a translational disorder (nematic-like) along the chain axis direction.

In the coexistence range, both Bragg reflections around $2\theta = 19°$ are broader. This implies that the two crystal phases coexist inside the crystallites and suggests that the nucleation of the new phase is easier than its growth through the individual crystallites.

To summarize, the phase transition induces a drastic reorganization of the microstructure related to the anisotropic volume change through T_c and to the order–disorder character of the structural change. From the diffraction data, the volumic expansion coefficient is about $1.3 \times 10^{-4}\ K^{-1}$ in the ferroelectric phase. It is much larger in the paraelectric phase ($5.3 \times 10^{-4}\ K^{-1}$), as is usual for disordered structures.

Of importance is the fact that, in the coexistence range, upon heating, the lattice parameters of the paraelectric phase a and b deviate from linear thermal expansion. This means that, upon heating, the first nuclei of the high temperature phase are compressed by about 2% in the matrix still predominantly in the ferroelectric phase (*Figure 3*). It is suggested that the corresponding internal pressure due to the first nuclei of the paraelectric phase raises T_c for the other crystals and hinders the growth of the high temperature phase. From measurements under hydrostatic pressure, the compressibility of the paraelectric phase is $2.5 \times 10^{-10}\ Pa^{-1}$ and T_c increases by $0.38\ K\ MPa^{-1}$ (Ref. 19). This enables the evaluation of the maximum internal pressure to be as high as 80 MPa and the corresponding shift of T_c to be about 30 K. It is shown in *Figure 5* that, upon heating, the transition first develops slowly and then more abruptly when the compression stress on the paraelectric lattice is released (*Figure 3*). This description is also supported by the narrowing of the temperature range of coexistence when the sample is cooled (15 K instead of 30 K). Then, the

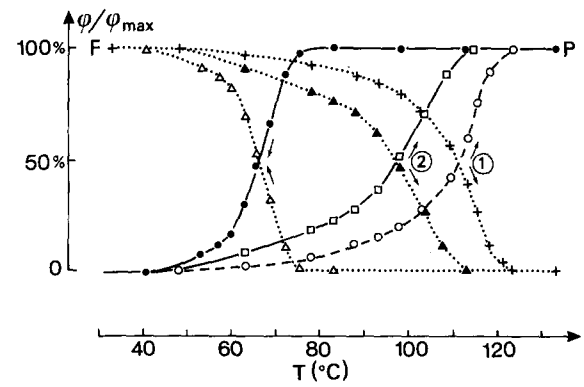

Figure 5 Relative contents of the ferroelectric, F, and of the paraelectric, P, phases *versus* temperature, T. ○ and +, First heating run; ● and △, cooling run; □ and ▲, second heating run

paraelectric crystals do not experience any compression from the matrix, except during the ultimate steps of the transition.

Other mechanisms may contribute to the spreading of T_c. First, due to the small crystal size, the local concentration of comonomers may fluctuate from one crystal to another and may be different from the average concentration upon which T_c is very sensitive. Second, there is a distribution of sizes of the lamellar crystals and, for the smaller crystals, the surface energy may be not negligible with respect to the volumic enthalpy change. Further evidence that T_c depends on the environment in which the structural transition takes place is given by the lowering of T_c in annealed samples.

Such shifts of the transition temperature as a function of the processing history have been recently reported[12] and were explained by a segregation of the VF_2 monomers out of the crystal lattice. However, for VF_2 contents larger than 60%, n.m.r. experiments have proved that the local concentration of comonomer units within the crystals is equal to the overall concentration within the chain[8]. It is more likely that the release of the internal stresses after a first cycle favours the transition to the disordered paraelectric phase.

SMALL ANGLE X-RAY SCATTERING

Results

The changes of morphology occurring in the course of the heating and cooling cycles can be determined by SAXS. Small angle X-ray scattering patterns of the copolymer at different temperatures are shown in *Figure 6*. They show a broad interference maximum arising from

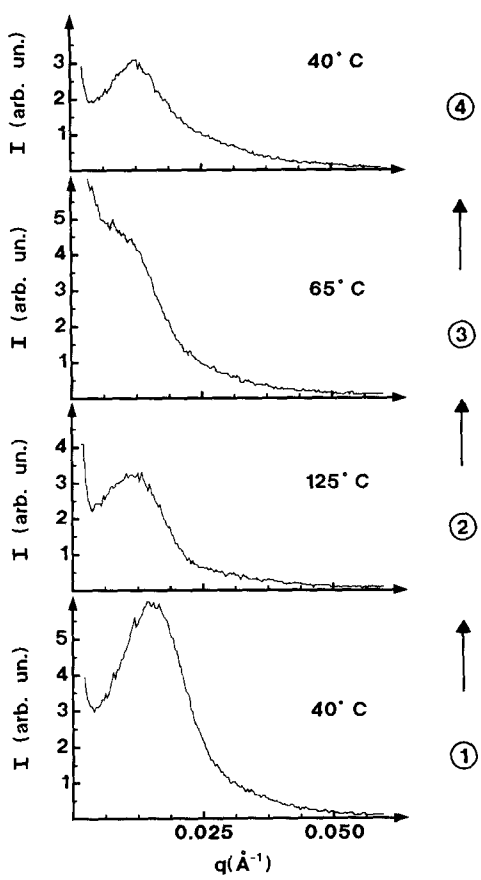

Figure 6 Small angle X-ray scattering patterns recorded at different temperatures (first temperature cycle)

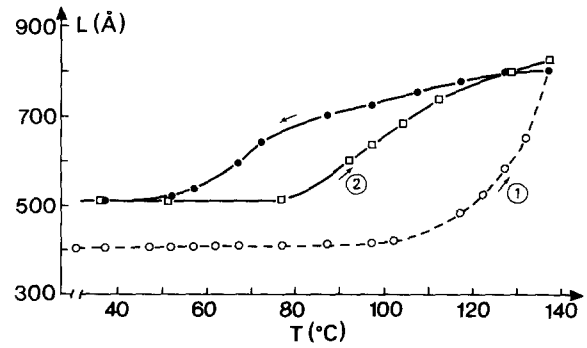

Figure 7 Variation of the long period, L, *versus* temperature, *T*. Symbols as in *Figure 4b*

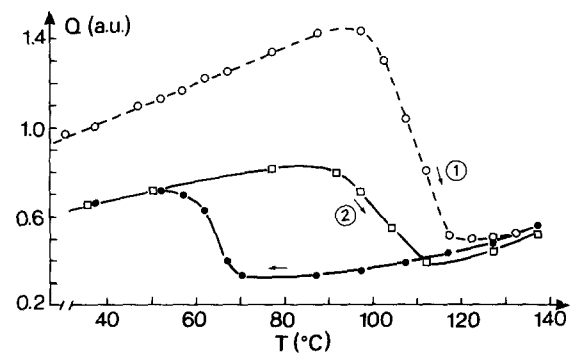

Figure 8 Temperature dependence of the invariant Q calculated from the integrated intensity scattered at small angles. Symbols as in *Figure 4b*

spatial correlation of lamellae with a rather constant thickness. Bragg's law has been applied to the value of the scattering vector q at the maximum intensity. It gives an estimate of the long period L. The variation of L as a function of temperature is shown in *Figure 7*. It appears that, during the first heating cycle, L drastically increases above T_c. Part of the change is reversible upon cooling through the transition and, as long as the temperature is not raised above the maximum temperature of the first cycle, a reversible variation of L takes place across the ferroelectric transition.

Additional information can be obtained from the so-called 'invariant' Q defined by:

$$Q = \int_0^\infty I(q) q^2 \, dq$$

Here, small angle scattering is caused by the presence of two phases, the amorphous and the crystalline phases, having different scattering densities (in a first approximation, each phase can be assumed to have a homogeneous electronic density). *Figure 8* shows the variation of Q during the two successive temperature cycles.

Without assumption on the shape or dimensions of the inhomogeneities the relationship between Q and the microstructural parameters (volume fractions of the crystalline and amorphous phases, ϕ_c and ϕ_a, densities of the crystalline and amorphous phases, ρ_c and ρ_a) can be written[13]:

$$Q \sim (\rho_c - \rho_a)^2 \phi_c (1 - \phi_c) = (\rho_c - \rho_a)^2 \phi_c \phi_a$$

From this expression, it appears that the variation of Q across the transition can be attributed to the change in ρ_c (see *Figure 3*), while the difference between the first and the second heating runs arises from the increase in

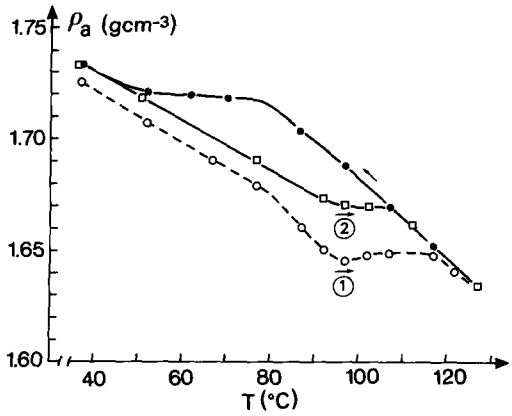

Figure 9 Density of the amorphous phase, ρ_a, as a function of temperature, T. Symbols as in *Figure 4b*

χ (see *Figure 4b*). However, a quantitative evaluation of the observed variation requires consideration of a three-phase system in the region of the ferroelectric transition.

For ternary systems, Q can be written:

$$Q \sim (\rho_{cF} - \rho_a)^2 \phi_{cF} \phi_a + (\rho_{cP} - \rho_a)^2 \phi_{cP} \phi_a + (\rho_{cF} - \rho_{cP})^2 \phi_{cF} \phi_{cP}$$

where ϕ_{cF} ϕ_{cP} and ρ_{cF}, ρ_{cP} correspond to the volume fractions and densities of the ferroelectric and paraelectric phases which can be evaluated from the WAXS data. From the above expression, one can thus derive the temperature dependence of the amorphous phase density, $\rho_a(T)$, from the integrated intensity at small angles, $Q(T)$. The results are presented in *Figure 9*. They show an unexpected compression of the amorphous phase when the crystal lattice is expanded (in the paraelectric phase). We have checked if this could be due to an inaccurate evaluation of χ: with the assumption of a reversible linear thermal expansion of the amorphous phase in the whole temperature range, the analysis of $Q(T)$ leads to non-physical variations of the crystalline volume fraction. If one further analyses the origin of the hysteresis in $\rho_a(T)$, it appears that, in the frame of a multi-phase model (with abrupt interfaces!), it is the only way to account for the strong decrease in $Q(T)$ across the ferroelectric transition. Physically, this means that ρ_a tends to be closer to the density of the paraelectric phase or, in other words, that the interface between the crystalline and the amorphous phase becomes less abrupt. It is clear that a model with a smooth density profile across the surface of the lamellae could also account for a smaller invariant in the paraelectric phase[17]. One must also note that the increase of the average ρ_a is consistent with the broadening of the amorphous halo towards the large angles observed in the paraelectric phase (*Figure 4a*).

From the values of χ and ρ_a at each temperature, we have calculated the volume expansion (and contraction) of the whole sample during the two successive cycles. The results are shown in *Figure 10a*. They compare fairly well with the measurements of the thermal expansion plotted in *Figure 10b*, and this provides confirmation of the results from X-ray measurements. The main difference between these two sets of data concern the first heating run. The difference could arise from a difference in the efficiencies of the quenching procedures which would result in different transition temperatures and in different contractions after annealing. However in the thermal expansion measurement, one must also consider a possible formation of voids, during the first temperature cycle, which would partly compensate the expected volumic contraction of the specimen after annealing.

Discussion

First temperature cycle. By comparing *Figures 7* and *8*, six regions can be distinguished:

(i) Region I (35–80°C). In the ferroelectric phase L stays constant ($L = 400$ Å) and Q increases linearly. As χ remains constant in this temperature range ($\chi = 0.65$) the increase in Q can be directly attributed to the thermal expansion of the amorphous matrix which causes a change in the density difference between the crystalline and the non-crystalline regions. This indicates a linear decrease of ρ_a from 1.725 to 1.675.

(ii) Region II (80–100°C). The onset of the Curie transition takes place at 80°C. From *Figure 7* it can be seen that the periodicity of the microstructure is not much changed at the beginning of the transition. This suggests that very fast crystallization upon quenching yields a constrained network of regularly stacked lamellae linked by amorphous chains which can cross different crystallites. The mobility should be very restricted by the interlamellar links and entanglements and reorganization is thus hindered.

One observes that in this temperature range Q keeps increasing and reaches a maximum around 95–100°C. This cannot be accounted for without considering a steeper decrease of the average ρ_a which could be attributed to the chain folds anchored at the surface of the lamellae undergoing the ferroelectric transition.

(iii) Region III (100–120°C). Above 100°C Q drops

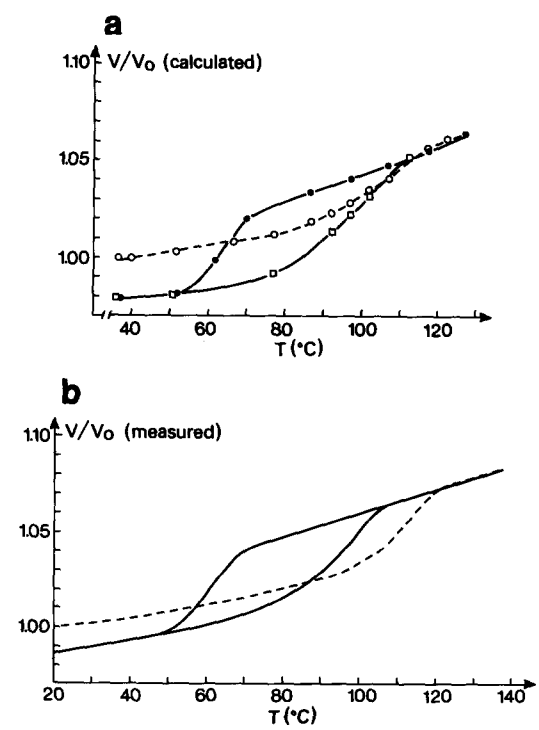

Figure 10 (a) Volume, V, expansion (and contraction) of a sample during two successive temperature cycles, calculated from the results presented in *Figures 3*, *4b*, *5* and *9*. Symbols as in *Figure 4b*. (b) Volume expansion of a similar specimen (0.59 g) recorded during two successive temperature cycles at a rate of ± 0.2 K min^{-1}

sharply. Obviously the fast decrease in Q is mainly due to the large variation of ρ_c across the ferroelectric transition: ρ_c drops from 1.96 g cm^{-3} in the ferroelectric phase to 1.83 g cm^{-3} in the paraelectric phase. The integrated intensity being proportional to $(\rho_c - \rho_a)^2$ can explain the observed ratio of 3 between the values of Q in the low and high temperature phases (with an almost constant $\rho_a = 1.65$).

Above 110°C L starts to increase. This increase occurs only when half of the crystalline phase has undergone the Curie transition. This confirms that the chain mobility, essential to enable the reorganization of the microstructure, is greatly enhanced in the paraelectric phase. The stresses are released. The plateau observed in $\rho_a(T)$ is probably related to the increase in crystallinity occurring mainly between 100°C and 130°C.

(iv) Region IV (120–140°C). The ferroelectric transition in the crystalline phase is completed and the sharp decrease in Q is followed by a slight and linear increase in the high temperature phase. This can be attributed to the normal thermal expansion of the amorphous phase (larger than that of the paraelectric phase).

A large shift of the SAXS peak position is observed above 120°C. The corresponding increase in L (from 500 to 800 Å) is too large to be accounted for by thermal expansion of the phases or by surface melting of the crystallites. Two possible explanations can be proposed. First, in the as-quenched specimen, the lamellar stacking involves lamellae having very different thicknesses. Thin crystals are intercalated between thick lamellae. At high temperatures lamellae thicken at the expense of the thinner crystals which melt. The diffusion of the chains between the amorphous and the crystalline regions is made easier by the high mobility of the chains. Thus the initial microstructure is replaced by one in which the spacing between centres of lamellae is greatly increased but the overall crystallinity is not much changed. This assumption is consistent with the small increase in χ, but one would also expect a reduction of the size distribution and therefore a narrowing of the correlation peak, while the opposite is observed. Second, the large anisotropy of the volume expansion during the Curie transition induces a twisting or a reorientation of some lamellae which is able to better accommodate the anisotropic expansion. For instance a local 'chevron' texture is able to minimize the anisotropy of the expansion of the whole specimen. This could be a second possible mechanism able to explain the observed increase in L together with the broadening of the correlation peak at small angles.

(v) Region V (140–75°C). Upon cooling, as long as the temperature is above 75°C, the integrated intensity decreases a little and the correlation peak gradually shifts to higher angles, reflecting a decrease in L. The non-linear decrease in Q can be explained by a linear contraction of the amorphous matrix plus a small increase in χ (see *Figure 4b*).

Nevertheless, it is not clear why L decreases. Intercalation of new, thin crystallites is a possible explanation consistent with the small increase in χ. It can also be suggested that the flattening of initially bent lamellae may contribute to this decrease.

(vi) Region VI (75–55°C). The Curie transition takes place in this temperature range. The mechanism of the transition seems to be very different upon cooling and upon heating. Indeed, upon cooling, the small angle diffraction maximum disappears at temperatures around 75°C and appears again at 60°C; the peak then lies at larger angles. The temporary disappearance of the interference maximum may be due to an intimate mixing of the two crystalline phases in the coexistence zone. If crystals of different densities (ρ_{cF} and ρ_{cP}) are randomly stacked the periodicity is destroyed and the interference maximum vanishes. On the contrary a fully developed SAXS peak remains visible when the Curie transition takes place upon heating suggesting a different nucleation and growth mechanism.

Finally, the first temperature cycle results in irreversible changes; the amorphous phase is a little more dense ($\rho_a = 1.735$); both L and χ are noticeably increased[15].

Second temperature cycle. The SAXS patterns exhibit the same evolution as those recorded during the first temperature cycle. It has to be pointed out that the increase in L, reflecting the change of the microstructure, is evident at 80°C. This supports the assumption that, in annealed samples, the reorganization in the vicinity of T_c is no longer hindered by internal stresses.

The changes in all the microstructural parameters are almost reversible and they take place during the phase transition. They are mainly related to the anomalous expansion (or contraction) of the crystal lattice and to the thermal expansion (or contraction) of the amorphous phase. More unexpected is the reversible change in χ. The results concerning L are puzzling. It must be stressed that, from one sample to another, the average L can vary over a large range, depending on the thermal and mechanical history of the sample. For example, before annealing L is 135 Å in a thin copolymer film cast using the spin coating technique[14]. In this case the average thickness of the lamellae, evaluated to be 80 Å, is related in a simple manner to L and χ ($= 0.6$) (one-dimensional model of stacking). Annealing above T_c increases L up to 310 Å and χ up to 0.8 while the lamellar thickness increases only by 20% (from the linewidth of the (0 0 1) Bragg reflection). As in the thick films presented in this paper, there is no correlation between L, the average thickness of lamellae and the crystallinity content. We suggest that after annealing there is no longer a regular stacking of parallel lamellae but instead another superstructure; L would therefore represent an average distance between the centres of mass of misoriented lamellae.

CONCLUSIONS

The main results obtained by WAXS and SAXS using SR can be summarized as follows: annealing of a quenched sample produces an increase in χ from 65 to 80%, and a reorganization of the microstructure taking place through the Curie transition upon heating as well as upon cooling. Subsequent heating and cooling cycles lead to reversible changes in the microstructure and in χ.

It appears that combination of WAXS ans SAXS, using the SR, is fruitful for *in situ* studies of phase transitions in semi-crystalline polymers.

These results have to be taken into account when considering the development of the wide range of applications of these new ferroelectric materials. Individual characteristics of the crystalline and amorphous phases both contribute to the resulting mechanical and piezoelectric properties of the material[14,16,18]. The control of χ and of the microstructure permits adjustable

physical properties. Thus, if one wants to achieve high piezoelectric coefficients, it is essential to control annealing procedures through the Curie transition.

ACKNOWLEDGEMENT

We are very grateful to the staff of LURE for their kind help during the experiments and especially to C. Williams, P. Vachette, O. Lyon, J. P. Benoit, M. Lemmonnier and P. Feder.

REFERENCES

1 Furukawa, T., Johnson, G. E., Bair, H. E., Tajitsu, Y., Chiba, A. and Fukada, E. *Ferroelectrics* 1981, **32**, 61
2 Lovinger, A. J., Davis, G. T., Furukawa, T. and Broadhurst, M. G. *Macromolecules* 1982, **15**, 23
3 Davis, G. T., Broadhurst, M. G., Lovinger, A. J. and Furukawa, T. *Ferroelectrics* 1984, **57**, 73
4 Tashiro, K., Takano, K., Kobayashi, M., Chatani, Y. and Tadokoro, H. *Ferroelectrics* 1984, **57**, 297
5 Tashiro, K., Takano, K., Kobayashi, M., Chatani, Y. and Tadokoro, H. *Polymer* 1984, **25**, 193
6 Petzelt, J., Legrand, J. F., Pacesova, S., Kamba, S., Kozlov, G. V. and Volkov, A. A. *Phase Transition* 1988, **12**, 305
7 Legrand, J. F., Schuele, P. J., Schmidt, V. H. and Minier, M. *Polymer* 1985, **26**, 1683
8 Hirshinger, J., Meurer, B. and Weill, G. *Polymer* 1987, **28**, 721
9 Legrand, J. F., Delzenne, P., Dianoux, A. J., Bee, M., Poinsignon, C., Broussoux, D. and Schmidt, V. H. *Springer Proc. Phys.* 1988, **29**, 59
10 Delzenne, P. *PhD Thesis* Grenoble Univ., 1986
11 Legrand, J. F., Delzenne, P. and Lajzerowicz, J. *IEEE Trans. Ultrason. Ferroelectrics and Freq. Control* 1986, **33**, 816
12 Green, J. S., Farmer, B. L. and Raboit, J. F. *J. Appl. Phys.* 1986, **60**, 2690
13 Feigin, L. A. and Svergun, D. I. In 'Structure Analysis by Small Angle X-ray and Neutron Scattering' (Ed. G. W. Taylor), Plenum Press, New York, 1987, p. 52
14 Legrand, J. F. *Ferroelectrics* 1989, **91**, 303
15 Fernandez, M. F., Susuki, A. and Chiba, A. *Macromolecules* 1987, **20**, 1806
16 Martinez-Salazar, J., Canalda Camara, J. C., Lopez Carbacos, E. and Balta Calleja, F. J. *Colloid Polym. Sci.* 1988, **266**, 41
17 Tsvankin, D. Ya. *Soviet Phys. Cryst.* 1969, **14**, 355
18 Kruger, J. K., Prechtl, M. and Legrand, J. F. *Ferroelectrics* 1990, **109**, 315
19 Legrand, J. F., Frick, B., Meurer, B., Schmidt, V. H., Bee, M. and Lajzerowicz, J. *Ferroelectrics* 1990, **109**, 321